Magnetic spin-flop transition and interlayer spin-wave dispersion in $PrCaFeO_4$ revealed by neutron diffraction and inelastic neutron scattering

N. Qureshi,[1,*] M. Valldor,[1,2] L. Weber,[1] A. Senyshyn,[3] Y. Sidis,[4] and M. Braden[1,†]

[1]*II. Physikalisches Institut, Universität zu Köln, Zülpicher Strasse 77, D-50937 Köln, Germany*

[2]*Max-Planck-Institut für Chemische Physik fester Stoffe, Nöthnitzer Str. 40, D-01187 Dresden*

[3]*Forschungs-Neutronenquelle Heinz Maier-Leibnitz (FRM-II), Technische Universität München, Lichtenbergstr. 1, D-85747 Garching near München, Germany*

[4]*Laboratoire Léon Brillouin, CEA/CNRS, F-91191 Gif-sur-Yvette Cedex, France*

(Received 10 February 2015; revised manuscript received 21 April 2015; published 2 June 2015)

We present a comprehensive study on $PrCaFeO_4$ using macroscopic methods, neutron and x-ray diffraction, as well as inelastic neutron scattering. One polycrystalline and two single-crystal samples were investigated exhibiting structural phase transitions from a high-temperature tetragonal phase to an intermediate orthorhombic phase (space group $Bmeb$) at 510 °C (783 K). At approximately 240 K a second structural phase transition takes place into the space group $Pccn$ where the tilt axis of the FeO_6 octahedra changes from the [100] to the ⟨110⟩ directions. Due to strong diffuse scattering at high temperatures neutron powder diffraction can only safely state that T_N is above 330 K. $PrCaFeO_4$ exhibits a magnetic spin-flop phase transition where the magnetic moments turn from the b axis to the c axis upon cooling. However, the transition temperatures and the width of this magnetic transition are strikingly different between the investigated samples, suggesting a strong influence from the real structure. Indeed, a significant difference in the oxygen content was deduced by single-crystal x-ray diffraction. The magnon dispersion was studied by inelastic neutron scattering revealing a nearest-neighbor interaction comparable to that in $LaSrFeO_4$ but with smaller anisotropy gaps. A clear interlayer dispersion was observed resulting from the structural distortions and the relief of geometrical frustration due to the orthorhombic splitting.

DOI: 10.1103/PhysRevB.91.224402 PACS number(s): 61.05.F−, 75.25.−j, 75.40.Gb

I. INTRODUCTION

$PrCaFeO_4$ is a member of the Ruddlesden-Popper transition-metal oxides series $R_{n+1}M_nO_{3n+1}$ (Ref. [1]), which has been intensively studied due to the large variety of interesting physical properties such as charge, spin, and orbital ordering. The fact that these order parameters are intimately coupled leads to complex physical properties and may result in fascinating phenomena like the colossal magnetoresistance in doped $LaMnO_3$ (Ref. [2]) ($n = \infty$, "113" structure) or high-temperature superconductivity. In comparison to the "113" perovskite, the "214" compound ($n = 1$) is a quasi-two-dimensional compound with a single-layered perovskite structure [see Fig. 1(a)]. The undistorted 214 compounds crystallize in the tetragonal space group $I4/mmm$, while smaller rare earth ions and the implied mismatch with the metal oxygen distances induce structural distortions associated with a tilt of the MO_6 octahedra. La_2CoO_4 (Ref. [3]) and La_2NiO_4 (Ref. [4]) contain MO_6 octahedra tilted around an axis parallel to an edge of the MO_6 octahedra which can be described within a low-temperature orthorhombic (LTO) phase with space group $Bmeb$. Both materials exhibit a further structural phase transition into a low-temperature tetragonal (LTT) phase (space group $P4_2/ncm$, where the octahedra are tilted around the M-O bonds) accompanied by a change in the magnetic structure.

Varying the occupation of the R site with three-valent ions (La, Y, or a rare earth) and two-valent earth-alkali ions results in structural modifications and complex phases, in which charge and orbital ordering is coupled to magnetic order. Typical examples are the stripe [5–7] or CE-type phases [8], which were extensively studied for M = Mn, Co, Cu or Ni. Very little is, however, known for the single-layered ferrates. $LaSrFeO_4$, in which Fe is three-valent with stable $3d^5$ configuration, exhibits G-type antiferromagnetic order with moments pointing along the iron-oxide layers [9–11]. $LaSrFeO_4$ shows strong Fe $3d$ to O $2p4$ hybridization which together with a strong e_g splitting explains the Mott-Hubbard character of the lowest dipole-allowed transition [12]. The strong hybridization also seems to cause the rather strong single-ion anisotropy effects, which cannot be expected for a pure high-spin $3d^5$ configuration [11]. The two related single-layered ferrates $NdSrFeO_4$ and $NdCaFeO_4$ were studied concerning their magnetic properties revealing a spin reorientation transition at low temperature [13,14].

Here, we present a comprehensive study on $PrCaFeO_4$ using diffraction and inelastic scattering techniques as well as macroscopic methods. In contrast to the closely related, but not isostructural compound $LaSrFeO_4$ (Ref. [11]), $PrCaFeO_4$ reveals an orthorhombic distortion which relieves the interlayer geometric frustration of this quasi-2D material. As a consequence interesting magnetic properties occur such as a spin-flop transition at rather high temperatures and a pronounced propagation of spin waves perpendicular to the Fe layers, which is rather uncommon in the layered 214 transition-metal oxides.

II. EXPERIMENTAL

The sample preparation was carried out similar to reported techniques on $LaSrFeO_4$ [10,15]. Powder samples of $PrCaFeO_4$ were prepared by mixing Pr_2O_3, $CaCO_3$, and Fe_2O_3

*Corresponding author: qureshi@ph2.uni-koeln.de

†braden@ph2.uni-koeln.de

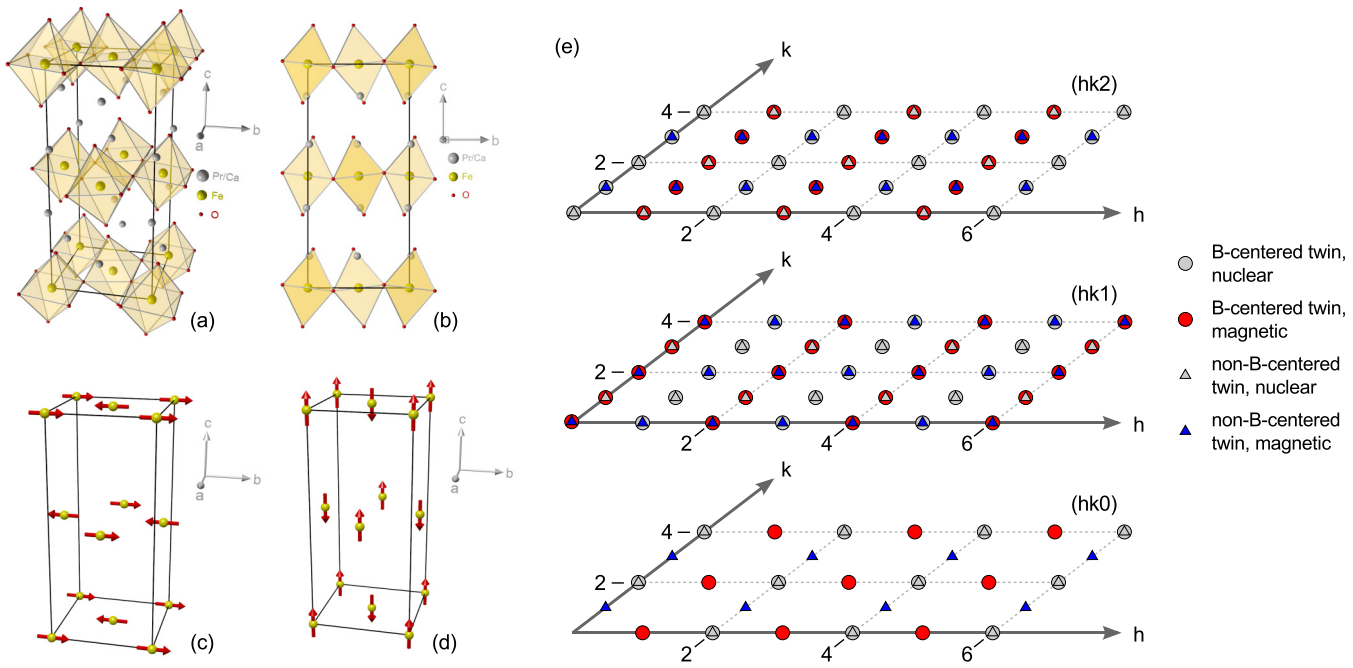

FIG. 1. (Color online) (a) Perspective view of the crystal structure of $PrCaFeO_4$ in space group $Bmeb$. (b) Orthographic view along the a axis emphasizing the tilt of the FeO_6 octahedra around the a axis. (c) High-temperature magnetic structure with the magnetic moments aligned along the b axis. (d) Low-temperature magnetic structure with $\mu \parallel c$. (e) Sketch of three reciprocal space planes for different l values clarifying the nuclear and magnetic zone centers of the B-centered twin (gray and red circles, respectively) as well as of the non-B-centered twin which is rotated by 90° around the c axis (gray and blue triangles, respectively).

in the stoichiometric ratio and sintering 100 h at 1200 °C. Diffraction patterns of all synthesized samples were taken on a Siemens D5000 x-ray powder diffractometer in order to confirm the correct phase formation (space group $Bmeb$). Large single crystals of $PrCaFeO_4$ were grown by the floating-zone method. For this purpose, $PrCaFeO_4$ powder was pressed into a cylindrical rod of 60 mm length and 8 mm diameter and sintered at 1300 °C for 20 h. One crystal (hereafter denoted as sample $S1$) was grown in a floating-zone furnace (Crystal Systems Incorporated) equipped with four halogen lamps (1000 W). The second crystal (hereafter denoted as sample $S2$) was grown in a Canon furnace with two halogen lamps of 2000 W where the molten zone is smaller due to better focusing properties. Both growth conditions were identical where the feed and seed rods rotated in opposite directions at about 10 rpm, while the molten zone was vertically moved at a growth speed of 3 mm/h. Both growths were performed in argon atmosphere under a pressure of 4.5 bar. The single crystal quality was checked by Laue precision photography. Suitable single crystals for x-ray diffraction were obtained by milling larger pieces in a ball mill for several hours. The characterization at the x-ray single crystal diffractometer Bruker Apex D8 confirmed the successful crystal growth. The magnetic structure was investigated at the neutron powder diffractometer SPODI (FRM-II, $\lambda = 1.55$ Å) using a powder sample (hereafter denoted as $S3$) in combination with a cryostat and a furnace in order to cover a large temperature range. Neutron diffraction experiments on single crystal $S2$ were performed on the three-axis spectrometer 3T1 (LLB, Saclay) to verify the magnetic structures. The same single crystal was then investigated by inelastic neutron scattering on the cold neutron spectrometer 4F2 (LLB, Saclay) where the low-energy part of the magnon dispersion was deduced along the main symmetry directions. Macroscopic properties were investigated using the single-crystal samples. All magnetization data were acquired with an MPMS-XL and a vibrating sample magnetometer (VSM) in a PPMS, both from Quantum Design (San Diego). The sample was held in place using an adhesive tape and a plastic straw, as supplied by the magnetometer manufacturer in the MPMS-XL, but was fastened with ceramic glue to a furnace in the VSM-PPMS. The high-temperature structural phase transition was investigated by single differential thermal analysis (SDTA) in a TGA/SDTA 851e (Mettler-Toledo), using a constant nitrogen flow and a platinum crucible. Electric resistivity has been measured by the standard four-point method.

III. NUCLEAR AND MAGNETIC STRUCTURE OF $PrCaFeO_4$

A. Macroscopic properties

Both single-crystal samples $S1$ and $S2$ were investigated concerning their macroscopic properties. SDTA measurements reveal an anomaly at 510 °C (783 K) indicating a structural phase transition as is shown in Fig. 2. The fact that both single crystals reveal an orthorhombic twinned structure (experimental proof shown in Sec. III D) at room temperature (RT) gives rise to the assumption of a high-temperature tetragonal (HTT) phase as for La_2NiO_4 (Ref. [4]). The magnetic susceptibility of $S1$ was investigated in a temperature range from 1.8 to 800 K revealing no sign of T_N owing to the strong two-dimensional character of the spin correlations (Fig. 3). The inset in Fig. 3 shows the high-temperature regime of the

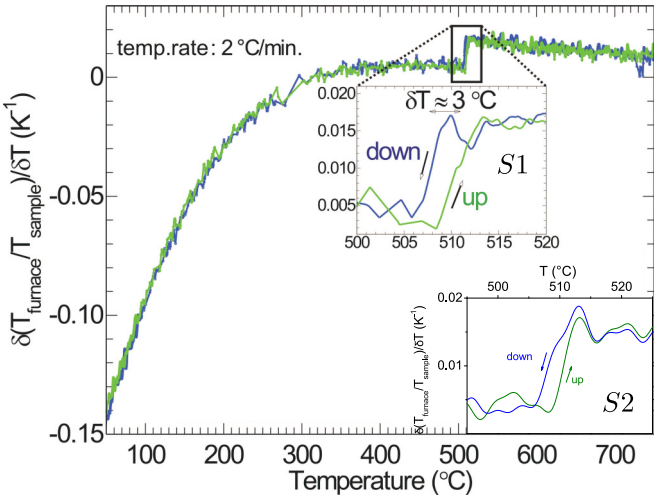

FIG. 2. (Color online) SDTA measurement of $PrCaFeO_4$ single crystals $S1$ and $S2$ revealing a structural phase transition from a high-temperature tetragonal phase to the orthorhombic structure below approximately 510 °C.

specific resistivity to which an Arrhenius function ($\ln\sigma = \ln\sigma_0 - \frac{\Delta}{2k_BT}$) was fitted resulting in a band gap of $\Delta = 0.36$ eV. In addition, sample $S2$ shows a pronounced anomaly at 42 K at low fields proving a magnetic phase transition (Fig. 4). A further anomaly can be observed at 255 K where an inflection point is present in the susceptibility curves for $B \perp c$. (Note that two orthorhombic directions perpendicular to the c axis have been measured, but the sample is in fact at least partially twinned, as discussed in detail in Sec. III D.) Above 255 K the in-plane susceptibilities $B \perp c$ are isotropic while a clear anisotropy can be observed below the inflection point, which can be explained by an imbalanced twin population.

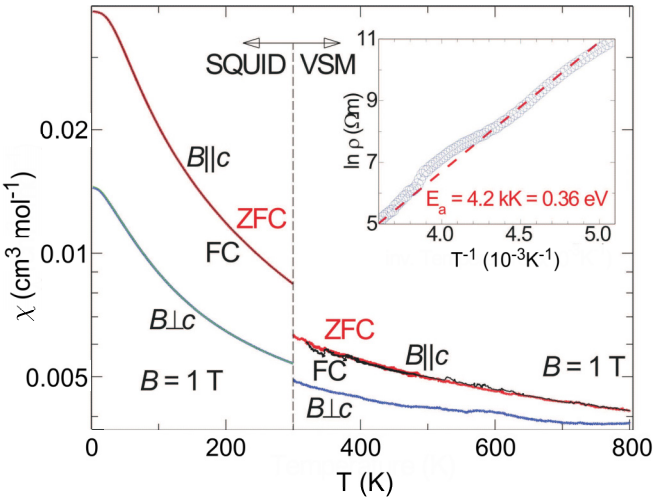

FIG. 3. (Color online) Magnetic susceptibility as a function of temperature measured on the single-crystalline sample $S1$ with the magnetic field of 1 T either parallel or perpendicular to the c axis. The inset shows the specific resistivity in an Arrhenius plot, from which the band gap of 0.36 eV was deduced.

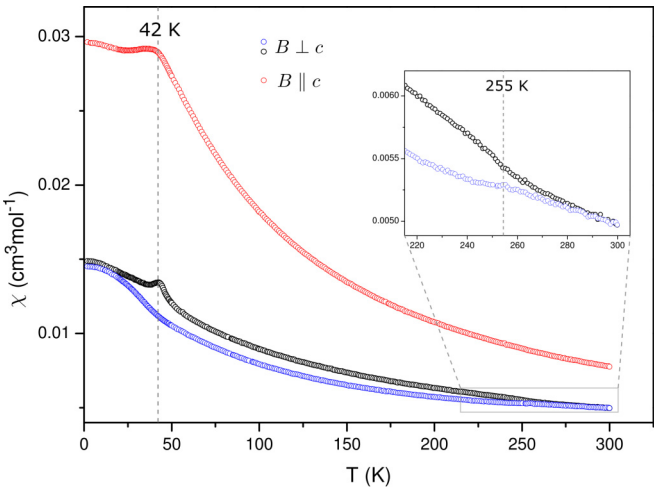

FIG. 4. (Color online) Magnetic susceptibility (field cooled) as a function of temperature measured on the single-crystalline sample $S2$ with a magnetic field of 10 mT parallel and perpendicular to the c axis (the latter corresponds to two orthorhombic in-plane axes of one twin). Besides the anomaly at 42 K, a less pronounced one is present at 255 K which is plotted on a smaller scale in the inset.

B. X-ray diffraction

We have investigated the nuclear structure of $PrCaFeO_4$ using x-ray diffraction on powder samples of $S1$ to $S3$. The RT diffraction pattern of $S1$ is shown in Fig. 5. All measured reflections could be indexed by the orthorhombic space group $Bmeb$. From Rietveld refinements on the powder samples we have derived the lattice constants at RT which are shown in Table I. It can be seen that the ground single crystals exhibit similar lattice constants, whereas the as-prepared powder sample deviates significantly with the a and b axis being smaller and the c axis being bigger. For a detailed investigation of the nuclear structure single-crystal data were used. More than 600 symmetry-independent reflections were measured

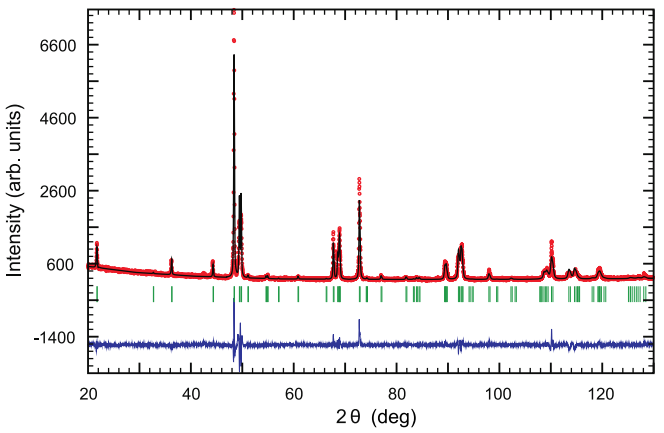

FIG. 5. (Color online) X-ray powder diffraction pattern of $PrCaFeO_4$ (sample $S1$) taken at RT with Cu K_α radiation. Raw data are depicted by (red) dots, while the calculated pattern and the difference line are represented by solid (black) and by solid (blue) lines, respectively. (Green) vertical bars indicate the position of Bragg reflections.

TABLE I. Lattice constants derived by x-ray powder diffraction on all three investigated samples. *S*3 is an as-grown powder sample, while *S*1 and *S*2 are ground single crystal samples.

	*S*1	*S*2	*S*3
a (Å)	5.4361(1)	5.434 43(8)	5.4251(2)
b (Å)	5.4855(2)	5.482 38(8)	5.4728(2)
c (Å)	12.1331(3)	12.1318(2)	12.1449(4)

which were then analyzed with the FULLPROF program [16] by refining the atomic positions, the anisotropic temperature factors, the occupation of the Pr/Ca and oxygen sites, as well as the extinction parameters (according to an empiric ShelX-like model [17]). The refined parameters are shown in Table II. The reliability factors of the refinements turn out to be excellent with $R_F = 2.5\%$ and $R_F = 1.7\%$ for *S*1 and *S*2, respectively. It can be seen that the atomic positions are the same within the error bars for both samples. Furthermore, the anisotropic temperature factors are comparable and the Pr:Ca ratio is close to 1:1. However, for *S*1 a significant oxygen deficiency is present on the O1 site, which is the basal oxygen of the FeO_6 octahedra mediating the magnetic superexchange.

C. Powder neutron diffraction

The nuclear and magnetic structures of $PrCaFeO_4$ (sample *S*3) were investigated between 4 K and RT by using a standard cryostat and between RT and 430 K inside a furnace. Neutron powder diffraction patterns were recorded in 15 K steps, which were then analyzed with the FULLPROF program. From all diffraction patterns the cell parameters (Fig. 6) were extracted by Rietveld refinements and plotted against the temperature (Fig. 6). At 300 K a pronounced anomaly is observable in the temperature evolution of the lattice parameters *a* and *b* (with no anomaly for *c*), where the system undergoes a structural phase transition. Following Ref. [4] the tetragonal space group $P4_2/ncm$ and the orthorhombic space group $Pccn$ were tested

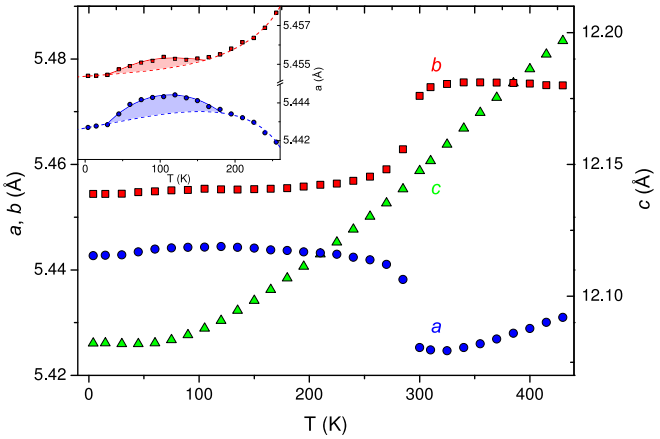

FIG. 6. (Color online) Lattice parameters of sample *S*3 (obtained by neutron powder diffraction) as a function of temperature clearly revealing a structural phase transition at 300 K. The inset shows an anomalous evolution of the in-plane lattice constants below 170 K. Note that the error bars are smaller than the height of a data point symbol.

TABLE II. Nuclear structure parameters within the *Bmeb* space group at RT as derived from the refinement to the single-crystal data. The first line of each entry refers to sample *S*1, the second line to sample *S*2. The extinction parameters according to an empirical Shelx-like correction are $x_{11} = 0.16(1)$, $x_{22} = 0.18(1)$, $x_{33} = 0.061(4)$ for *S*1 and $x_{11} = 0.10(1)$, $x_{22} = 0.078(9)$, $x_{33} = 0.032(2)$ for *S*2.

	Pr/Ca	Fe	O1	O2
x	0	0	0.25	0
	0	0	0.25	0
y	0.009 90(2)	0	0.25	− 0.0470(5)
	0.010 02(2)	0	0.25	− 0.0471(5)
z	0.357 71(1)	0	− 0.9869(2)	0.1727(2)
	0.357 70(1)	0	− 0.9869(2)	0.1728(2)
occ	0.494(3)/0.506(3)	1	0.95(1)	1.03(1)
	0.509(3)/0.491(3)	1	1.06(1)	1.04(1)
U_{11} (Å^2)	0.006 79(7)	0.0009(1)	0.0033(5)	0.043(2)
	0.008 27(7)	0.0022(1)	0.0068(5)	0.044(2)
U_{22} (Å^2)	0.006 25(7)	0.0010(1)	0.0039(4)	0.0188(9)
	0.007 90(8)	0.0026(2)	0.0067(5)	0.0201(9)
U_{33} (Å^2)	0.002 16(7)	0.0171(2)	0.0171(7)	0.0032(5)
	0.004 02(7)	0.0188(2)	0.0222(8)	0.0057(6)
U_{12} (Å^2)	0	0	− 0.0033(4)	0
	0	0	− 0.0035(4)	0
U_{13} (Å^2)	0	0	0	0
	0	0	0	0
U_{23} (Å^2)	0.000 54(3)	− 0.0006(1)	0	− 0.0004(5)
	0.000 54(3)	− 0.0006(1)	0	− 0.0004(5)

TABLE III. Basis vectors ψ of the irreducible representations Γ_{LTO} (low-temperature orthorhombic phase, $Pccn$), Γ_{ITO} (intermediate-temperature orthorhombic phase, $Pccn$) and Γ_{HTO} (high-temperature orthorhombic phase, $Bmeb$) for the Fe^{3+} ions at given fractional coordinates (x, y, z) associated with a propagation vector $\mathbf{q} = (1,0,0)$. The components u, v, and w connected to the spin S_{Γ}^{r} were refined according to their constraints (an overline indicates a negative number).

Atom r	(x, y, z)	ψ_{LTO}	ψ_{ITO}	ψ_{HTO}
1	$(0, 0, 0)$	$\begin{pmatrix} u \\ v \\ w \end{pmatrix}$	$\begin{pmatrix} u \\ v \\ w \end{pmatrix}$	$\begin{pmatrix} 0 \\ v \\ w \end{pmatrix}$
2	$(\frac{1}{2}, \frac{1}{2}, 0)$	$\begin{pmatrix} u \\ v \\ \overline{w} \end{pmatrix}$	$\begin{pmatrix} \overline{u} \\ \overline{v} \\ w \end{pmatrix}$	$\begin{pmatrix} 0 \\ \overline{v} \\ w \end{pmatrix}$
3	$(0, \frac{1}{2}, \frac{1}{2})$	$\begin{pmatrix} u \\ \overline{v} \\ w \end{pmatrix}$	$\begin{pmatrix} \overline{u} \\ v \\ \overline{w} \end{pmatrix}$	$\begin{pmatrix} 0 \\ v \\ \overline{w} \end{pmatrix}$
4	$(\frac{1}{2}, 0, \frac{1}{2})$	$\begin{pmatrix} u \\ \overline{v} \\ \overline{w} \end{pmatrix}$	$\begin{pmatrix} u \\ \overline{v} \\ \overline{w} \end{pmatrix}$	$\begin{pmatrix} 0 \\ \overline{v} \\ \overline{w} \end{pmatrix}$

on the data obtained below 285 K, and the agreement is better than with space group $Bmeb$ in both cases. Due to the larger number of free parameters, the refinement with space group $Pccn$ yields a slightly better agreement ($R_F = 3.61\%$) than $P4_2/ncm$ ($R_F = 3.93\%$), however the difference is marginal. Constraining $a = b$ within $Pccn$ yields an agreement factor of $R_F = 3.71\%$. As the R values are similar it cannot fully be excluded that the observed orthorhombicity at LT might be an artifact of the refinement process. Below 170 K a further anomalous behavior of the in-plane lattice constants can be observed (see inset of Fig. 6) which will be discussed later in the text. The comparison between HT and LT data results in strong additional intensities at positions forbidden by the nuclear space group, but still compatible with the lattice periodicity, indicating a propagation vector $\mathbf{q} = (100)$. Three reflections could not be indexed with the $PrCaFeO_4$ structure. Those impurity reflections at scattering angles of approximately 20°, 23°, and 39° could be indexed with the space group $Pbnm$ corresponding to the perovskite compound $PrFeO_3$ (with a volume fraction of 8%).

The symmetry analysis was done using the BASIREPS program included in the FULLPROF package. Four irreducible representations are compatible with the $Bmeb$ space group, $\mathbf{q} = (100)$ and a magnetic ion at the position (0,0,0), from which only one was able to explain the HT data for which the nuclear structure is described in space group $Bmeb$ (listed as Γ_{HTO} in Table III with the basis vectors). The magnetic structure corresponds to a collinear alignment parallel to the orthorhombic b axis with a ferromagnetic arrangement within the b-c plane and alternation along the a direction (note that the magnetic structure is qualitatively the same as in the $LaSrFeO_4$ compound [11]). The lower symmetry in $PrCaFeO_4$ allows for a weak canting of the moments to the c direction which is ferromagnetic within a single plane but antiferromagnetic between them. However, this

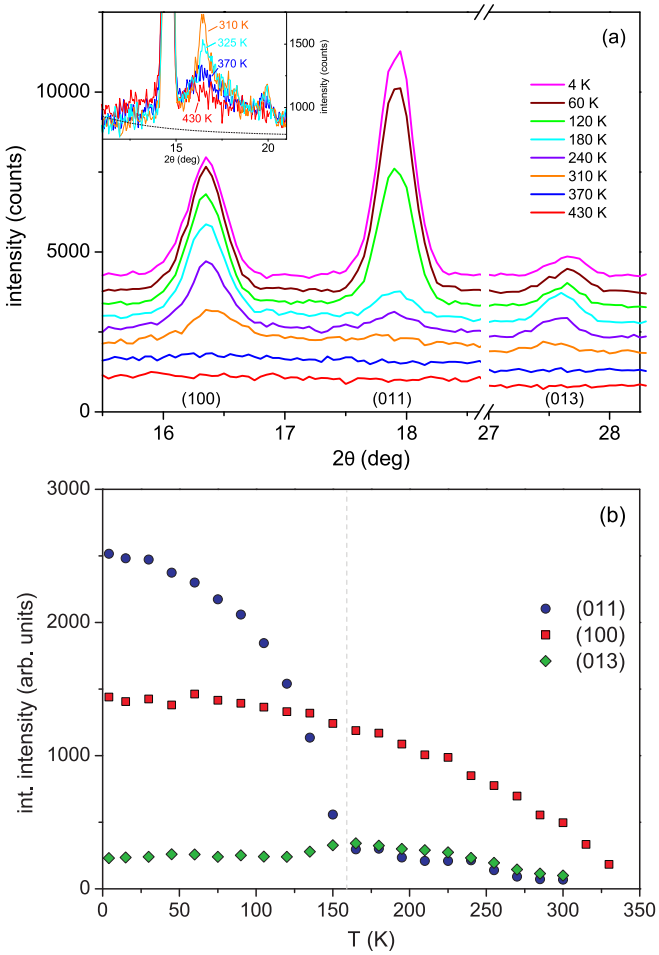

FIG. 7. (Color online) (a) Two sections of the diffraction patterns taken at different temperatures focusing on the magnetic reflections (100), (011), and (013). The inset shows two high-temperature diffraction patterns revealing very broad reflections owing to strong diffuse magnetic scattering. (b) Integrated intensities of the magnetic Bragg reflections shown in (a). While the intensity of the (100) reflection does not show any anomalies, the (011) increases and the (013) decreases in intensity at approximately 160 K. The data were obtained from sample $S3$ on SPODI.

weak canting cannot be observed experimentally. Figure 7(a) shows two sections of the diffraction patterns taken at various temperatures focusing on three purely magnetic peaks [(100), (011), and (013)] that are isolated from other reflections. The inset in Fig. 7 shows the strong diffuse scattering persisting up to 420 K which does not allow a clear determination of T_N. The integrated intensities are depicted in Fig. 7(b) as a function of temperature.

No anomalies in the magnetic scattering could be observed when passing the $Bmeb \rightarrow Pccn$ structural phase transition slightly below 300 K. Therefore, the magnetic structure must remain essentially unchanged within the intermediate-temperature (IT) range phase, i.e., it must be compatible with Γ_{HTO}. Because the analysis of the nuclear structure slightly favors space group $Pccn$ we also describe the magnetic structure in this symmetry. The basis vector of the irreducible representation labeled as Γ_{ITO} (see

Table III) is identical to that of Γ_{HTO} besides an additional x component of the ordered moment. In the $Pccn$ Γ_{ITO} phase moments cant also in the a-b planes. This magnetic structure is able to explain the IT range between 160 and 300 K. Obviously, the (011) reflection significantly gains intensity when cooling below 160 K, while the (013) reflection becomes weaker. On the other hand the (100) shows no effect. Taking into account the simple neutron selection rule that only moments perpendicular to the scattering vector contribute to the magnetic intensities, these observations suggest a spin rotation from the b axis to the c axis upon cooling. At LT the magnetic Bragg intensities cannot be described by the same irreducible representation as at higher temperatures (both in space group $Pccn$). Instead, for the LT data the irreducible representation Γ_{LTO} (see Table III) was used in which the z component of the magnetic moments transforms in the same way as the y component in Γ_{ITO}. This structure reflects thus the same Heisenberg interaction parameters just with a different orientation of the collinear moments. Again, this symmetry allows for canting of the moments and even yields a ferromagnetic contribution in the x direction, which can be associated with the low temperature anomaly in the in-plane susceptibility (see Fig. 4). The observed and calculated diffraction patterns are visualized in Fig. 8 for $T = 4$ K ($R_{F,\mathrm{mag}} = 12.1\%$) and $T = 180$ K ($R_{F,\mathrm{mag}} = 11.2\%$).

As can be seen from Fig. 7 the magnetic phase transition associated with the spin reorientation is continuous and extends over a temperature range of 100 K. Apparently fractions of the sample volume locally undergo the magnetic phase transition at different temperatures in accordance with the first-order character of the transition. An inhomogeneous distribution of the O1 vacancies may explain this effect. All diffraction patterns could be explained by a phase coexistence of two magnetic structures corresponding to Γ_{LTO} and Γ_{ITO} with the magnetic moment and the volume fraction of the respective phases as refined parameters.[1] The refined values show an expected smooth increase of the magnetic moment [comparable to the integrated intensity of the magnetic (100) reflection] and a transition regime from roughly 175 to 75 K as deduced from the volume fraction of the magnetic phases (Fig. 9).

The magnetic phase transition is decoupled from the structural $Bmeb \rightarrow Pccn$ transition associated with the octahedron tilting. Nevertheless the spin reorientation is connected to the lattice as is indicated by the anomalous behavior of the lattice constants a and b within the transition regime (see Fig. 6). In fact, a tetragonal constraint on the lattice constants results in a similar anomaly of a in the same temperature range. In Fig. 10, the FeO_6 octahedron tilting angle is plotted as a function of temperature yielding a small continuous increase upon cooling, which might modify the spin-orbit coupling and favor a spin alignment along the c axis.

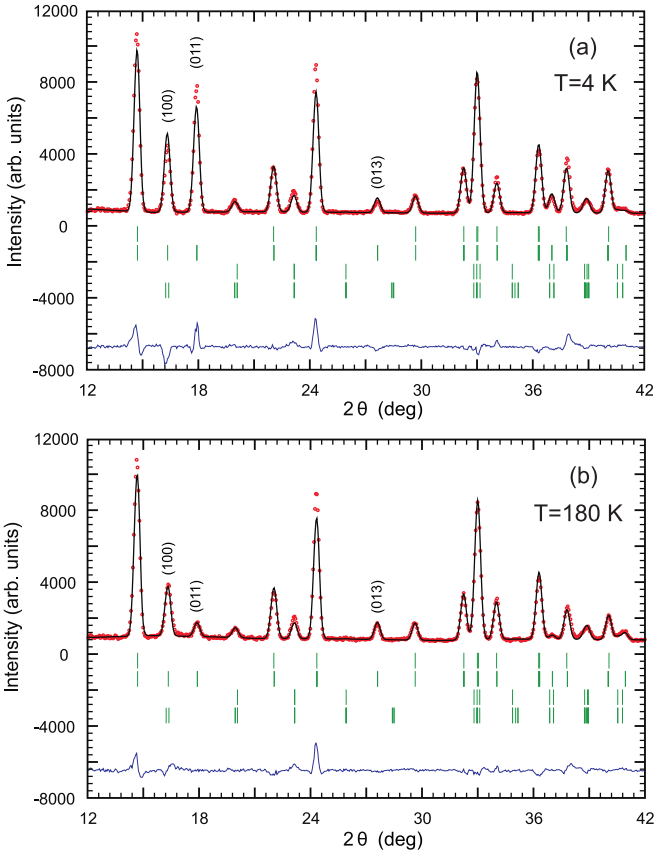

FIG. 8. (Color online) Neutron powder diffraction patterns of sample $S3$ taken at (a) $T = 4$ K and (b) $T = 180$ K. Raw data are depicted by (red) dots, while the calculated pattern and the difference line are represented by solid (black) and by solid (blue) lines, respectively. (Green) vertical bars indicate the position of Bragg reflections of $PrCaFeO_4$ (first line for nuclear, second line for magnetic structure) and $PrFeO_3$ (third line for nuclear, fourth line for magnetic structure).

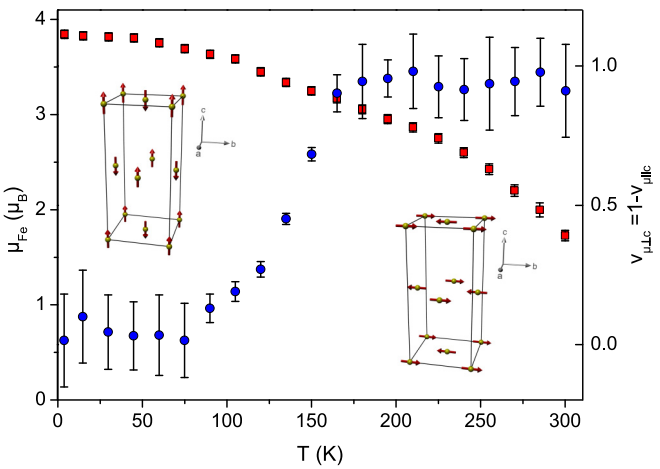

FIG. 9. (Color online) Temperature dependence of the size of the magnetic moment [(red) squares, left abscisse] and the volume fraction $v_{\mu\perp c}$ [(blue) dots, right abscisse] of the magnetic phase with $\mu \perp c$ ($v_{\mu\perp c} = 1\text{-}v_{\mu\parallel c}$) in sample $S3$. The respective magnetic structures correspond to antiferromagnetically coupled spin within the a-c plane with alternating spin direction along the b axis.

[1]Note that a continuous spin rotation in a homogenous phase would produce exactly the same diffraction patterns, however a magnetic moment configuration between the b and the c axis reveals a reduced magnetic symmetry in comparison to the initial and final phases, for which this scenario is rather unlikely.

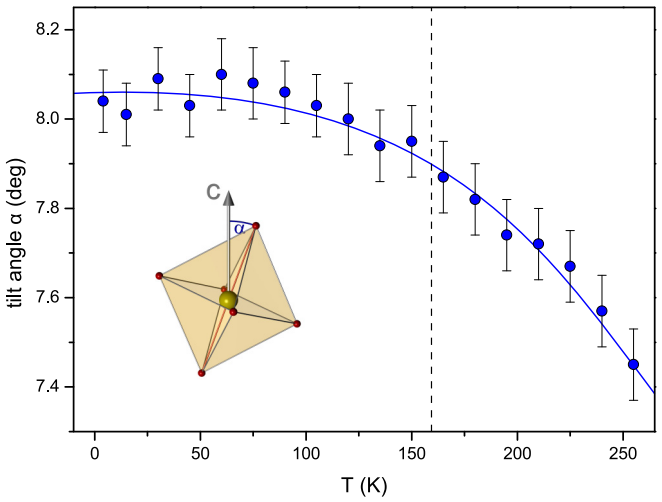

FIG. 10. (Color online) Octahedra tilt around the Fe-Fe bond within the LTT phase (measured on sample $S3$) expressed by the angle between the octahedra axes and the c axis as a function of temperature. The dashed line marks the onset of the magnetic phase transition as seen in Fig. 7(b).

D. Single-crystal neutron diffraction

The single crystal $S2$ was investigated at the three-axis diffractometer 3T1 (LLB, Saclay). The crystal was mounted in the [100]-[001] scattering plane giving access to ($h0l$) reflections. However, due to the twinned nature of the sample ($0kl$) reflections are superimposed [see Fig. 1(e)]. Figure 11 shows the temperature dependence of the integrated intensities of different nuclear and magnetic reflections. In Fig. 11(a) a clear anomaly in the temperature dependence of the (200) reflection can be observed at roughly 240 K, while no such anomaly is visible for the (006) reflection. Compared to the powder data this can be attributed to the structural phase transition into the ITO phase with space group $Pccn$. In Figs. 11(b) and 11(c) special reflections are shown which prove the twinned state of the single crystal. Figure 11(b) depicts three purely magnetic reflections where only one of the twin orientations contributes to the respective intensities.[2] The comparison of the various intensities indicates that both twin domains exist in the crystal, but that there is a pronounced preference of the B-centered domains (twin I). The temperature dependence of each reflection is qualitatively the same as the one in Fig. 7 therefore confirming the magnetic phase transition from an in-plane to an out-of-plane spin configuration with decreasing temperature.[3] However, the spin-reorientation transition observed in $S2$ sets in at lower temperature and is sharper compared to the neutron powder data of $S3$, which strengthens the assumption of a real structure effect on the magnetic phase transition temperature. Two further reflections were investigated which

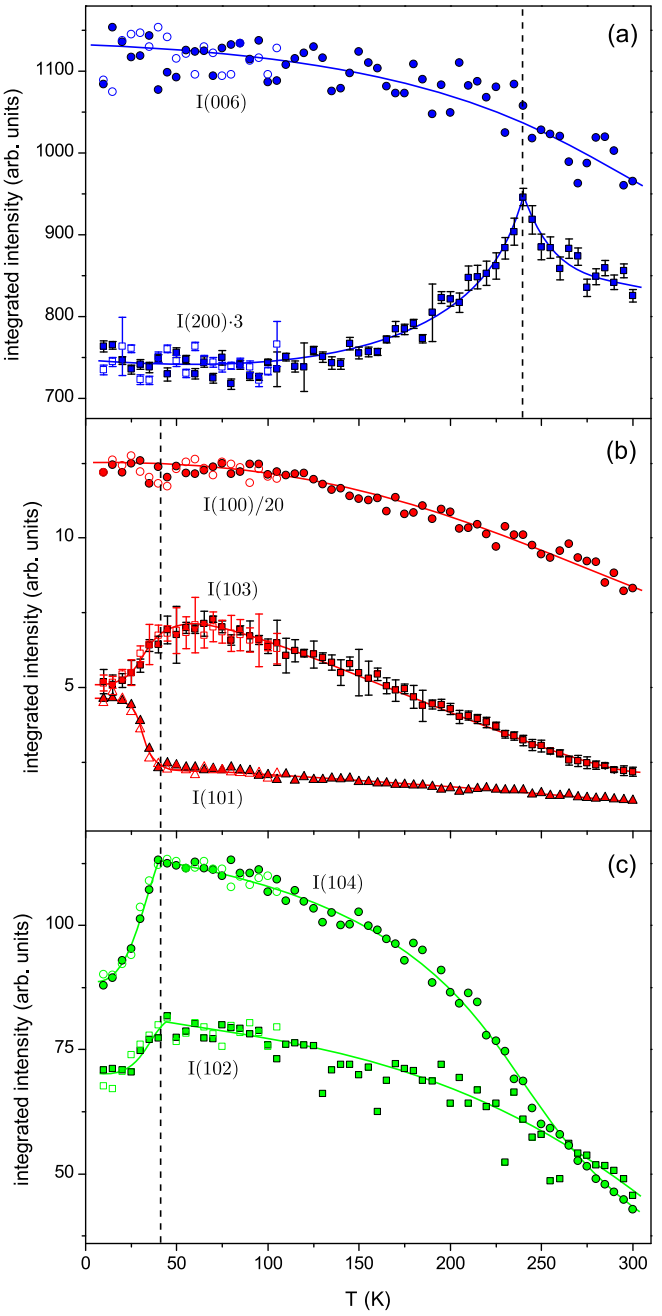

FIG. 11. (Color online) Temperature dependence of (a) pure nuclear reflections, (b) pure magnetic reflections, and (c) reflections with both nuclear and magnetic contribution due to the twinned sample. In order to improve visibility some intensities were multiplied by a factor as shown within the plots. Filled symbols were recorded upon cooling while open symbols were recorded on heating. Phase transitions are marked with dashed lines.

have both nuclear and magnetic contributions from the two twins [Fig. 11(c)] as can be deduced from the anomaly at the magnetic phase transition temperature and from the relatively strong intensity at HT compared to the pure magnetic reflections of (b). The measured intensities are composed of the magnetic (102) and (104) reflections as well as of the nuclear (012) and (014) reflections stemming from the non-B-centered domains (twin II). All integrated intensities were recorded

[2]The (010), (103), and (101) are forbidden nuclear and forbidden magnetic reflections in the $Bmeb$ structure with $\mathbf{q} = (100)$, while the (100), (013), and (011) are allowed by magnetic symmetry.

[3]Note that the hkl multiplicity factor, an unequal magnetic domain population, and different absorption conditions due to the sample orientation may explain the different intensity ratios between the magnetic peaks recorded on the powder and the single-crystal sample.

upon cooling and heating across the magnetic phase transition, which yielded no indication for a temperature hysteresis.

E. Discussion of the magnetic structure in $PrCaFeO_4$

Strong coupling between the magnetic moments and the lattice can only be explained by the microscopic spin-orbit coupling. One may therefore expect only a weak coupling for the ideal high-spin $3d^5$ configuration with zero orbital moment. There is, however, strong evidence for Fe $3d$ to O $2p$ hybridization [12], which will allow for finite spin-orbit coupling effects in these ferrates. Because the spin-orbit effects remain weaker than in systems with stronger orbital moment, the induced single-ion anisotropy energies will also be weak resulting in nearly degenerate states with the same antiferromagnetic scheme but different alignment of the magnetic moments. Indeed spin-reorientation transitions are well known in the perovskite orthoferrates, $R\mathrm{FeO_3}$ [18–20]. In the single-layered ferrates the spin reorientation is only observed when the crystal structure is considerably distorted [13,14]. Because the different spin arrangements are nearly degenerate, the real structure can have a strong impact on the spin reorientation transition as we observe it between samples $S2$ and $S3$. In the less distorted material $LaSrFeO_4$ the quenching of the orbital moment must be weaker so that the magnetic anisotropy is better defined. It has been speculated that the spin reorientation is triggered by the ordering of the R site [13,14], but the observation of this transition in $PrCaFeO_4$ at high temperature clearly shows that the spin reorientation is an intrinsic effect of the Fe lattice.

For a layered material one may expect a magnetic easy axis perpendicular to the layers or an easy plane parallel to them. The finding of magnetic moments pointing either along or perpendicular to the planes is thus astonishing and points to a peculiar orbital arrangement. This perpendicular easy plane is a direct consequence of the orthorhombic distortion. The same situation has been observed for the FeAs-based materials of type $BaFe_2As_2$, which are also layered and tetragonal in their undistorted form [21]. In spite of an only small orthorhombic distortion in their antiferromagnetic phase, these materials with ordered moment parallel to the FeAs layers exhibit a hard magnetic axis perpendicular to the moment but parallel to the FeAs layers (or an easy plane perpendicular to the layers) [22]. Again in close resemblance to the 214 ferrates, a spin-reorientation transition from an in-plane to an out-of-plane configuration of the magnetic moments occurs in Na-doped $BaFe_2As_2$ with stronger structural deformations [23].

The neutron powder diffraction experiments reveal a small and continuous increase of the tilting angle upon decreasing temperature (see Fig. 10). The octahedral tilt together with the temperature-dependent evolution of the lattice constants governs the interplay between spin-orbit coupling and magnetostriction, which results in the spin-flop transition.

IV. MAGNON DISPERSION IN $PrCaFeO_4$

The magnon dispersion was investigated at the 4F2 spectrometer ($\mathbf{k}_f = 1.55$ Å^{-1}) along the principal crystallographic directions at 10 K ($\mu \parallel c$) and 60 K ($\mu \perp c$) in the [100]-[010] and in the [100]-[001] scattering planes using the single-crystal sample $S2$. The limited accessible bandwidth of the magnon dispersion along the [ξ00] and [0ξ0] directions (note that the magnon dispersion in $LaSrFeO_4$ extends to energy transfers of 70 meV) only allows an estimate of the in-plane exchange parameters. In order to obtain the most reliable results all data were analyzed by folding the magnon cross section with the instrument resolution at each data point using the RESLIB code [24]. Furthermore, all constant-energy or all constant-**Q** scans measured under the same conditions were fitted by globally refining the exchange parameters, a single scale factor, and the background. The magnon dispersion was derived within linear spin-wave theory using a Hamiltonian of a Heisenberg antiferromagnet with isotropic nearest-neighbor interaction (J_1, connecting two nearest-neighbor antiferromagnetically coupled spins within the a-b plane), interplane interaction [J_c, connecting two antiferromagnetically coupled spins at (0,0,0) and (0.5,0,0.5)], and an effective magnetic anisotropy field H_A along the z axis. In a tetragonal material like $LaSrFeO_4$ the interlayer coupling is fully frustrated, but due to the orthorhombic distortion the pairs (0,0,0)/(0.5,0,0.5) and (0,0,0)/(0,0.5,0.5) are no longer equivalent. The diagonalization of the Hamiltonian [25] leads to the dispersion relation

$$\hbar\omega_q = \{[4S(J_1 + J_c) + g\mu_B H_A]^2 - [4S(J_1 \cos\pi q_x \cos\pi q_y + J_c \cos\pi q_x \cos\pi q_z)]^2\}^{\frac{1}{2}}. \quad (1)$$

A global refinable scale factor was used including the magnetic form factor, the Bose factor, and a $1/\omega$ term in order to account for the energy and **Q** dependence of the magnetic scattering. The background was treated with an energy-dependent polynomial function of second order. Figure 12 shows all constant-energy scans taken at $T = 10$ K in the [100]-[010] scattering geometry. The solid lines are the result of the global fit of the magnon cross section to raw data, where only J_1, a single scale factor, the Lorenzian energy half width (HWHM) of the magnon mode, and three background parameters were refined. The agreement of the refined magnon cross section (convoluted with the resolution function) with the observed data is excellent and even the characteristics of the peak shapes are well reproduced. Constant-**Q** scans at $\mathbf{Q} = (100)$ were performed within both magnetic phases (Fig. 13) and clearly exhibit the higher gap value at 60 K. As can be seen in the constant-**Q** scan at 60 K (Fig. 13) the scattered intensity is considerably higher at energies below 5 meV, which can entirely be explained by the Bose factor meaning that the refinable scale factor is of the same order for all analyzed temperatures. By fitting the macroscopic cross section to raw data in Fig. 13 and fixing the previously obtained parameter J_1, the anisotropy field H_A was derived. Again the convoluted cross section agrees very well with raw data. This procedure was continued iteratively until both constant-energy and constant-**Q** scans were described by the same set of J_1 and H_A parameters. Note that a global fit including both kinds of scans was not possible due to the inaccurate description of the resolution ellipsoid at small energy transfers that had to be compensated by the Lorenzian energy half width.

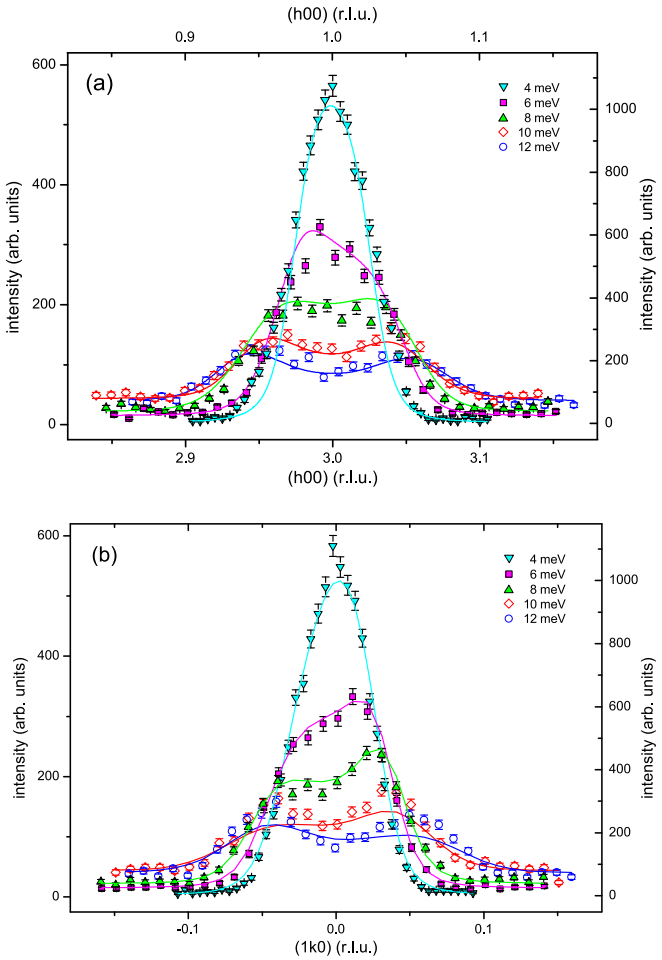

FIG. 12. (Color online) Constant-energy scans along the (a) [ξ00] and (b) [0ξ0] directions. The solid lines are the results of the global fit of the convoluted magnon cross section to raw data. Energy transfers of 4, 6, and 8 meV were measured at (100)+**q** (intensity corresponding to right ordinate), while energy transfers of 10 and 12 meV were measured at (300)+**q** (intensity corresponding to left ordinate).

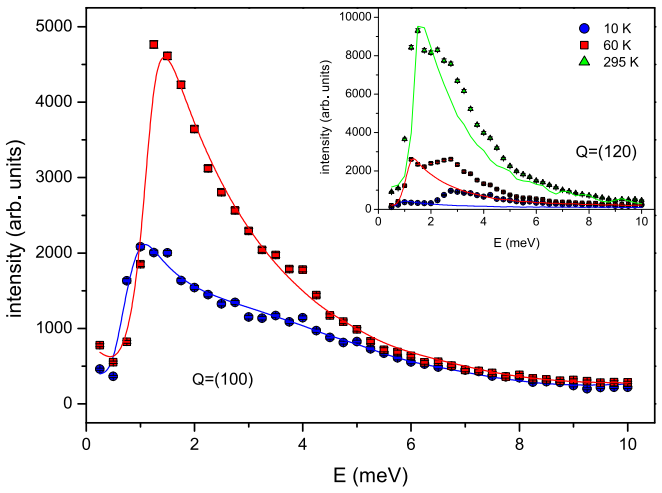

FIG. 13. (Color online) Constant-**Q** scans at the magnetic zone center (100) revealing an anisotropy gap of 0.6(1) meV. The inset confirms a phononic signal which decreases in relative intensity to the total signal with increasing temperature due to the Bose factor.

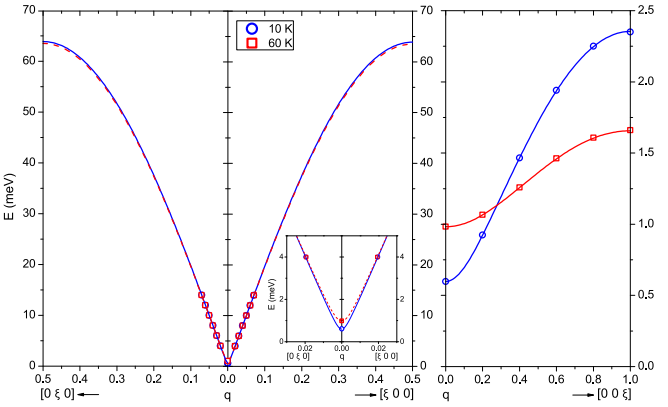

FIG. 14. (Color online) Magnon dispersion in $PrCaFeO_4$ along the main orthorhombic symmetry directions at $T = 10$ K [(blue) circles] and $T = 60$ K [(red) squares].

Assuming $S = 2.5$ the refined parameters at $T = 10$ K are $J_1 = 6.39(2)$ meV and $\mu_B H_A = 0.002(1)$ meV. These values were used with Eq. (1) in order to compute the peak positions of each scan shown together with the dispersion curve in Fig. 14. The value of the anisotropy gap amounts to 0.6(1) meV. The same analysis procedure was employed for the 60 K data yielding $J_1 = 6.35(2)$ meV, $\mu_B H_A = 0.004(1)$ meV, and a larger gap value of 1.0(1) meV. The values of the spin gaps in both phases and the corresponding anisotropy terms in the Hamiltonian are small, as is expected for the $3d^5$ configuration of Fe^{3+}, and they are even smaller than the out-of-plane gap in $LaSrFeO_4$ which agrees with spin reorientation occurring only in $PrCaFeO_4$. So far we neglect the partial twinning of the crystal as the only parameter breaking the tetragonal symmetry is J_c which does not possess a strong impact for the in-plane dispersion. Therefore, the magnon dispersions along [ξ 0 0] and [0 ξ 0] are almost similar and there is no difference between the two phases.

The crystal was then remounted with [100]-[001] defining the scattering plane in order to investigate the c dispersion. Due to the expected weakly dispersive mode along [0 0 ξ], only constant **Q** were performed (Fig. 15) which reveal a finite interaction between the vertically separated FeO planes expressed by $J_c = 0.002(1)$ meV at 10 K ($J_c = 0.001(1)$ meV at 60 K). Compared to Fig. 13 the magnon peak is suppressed as now the steep in-plane dispersion is folded with the relaxed vertical Q resolution of a focusing triple-axis spectrometer. The transversal magnon disperses from the magnetic zone center at (100) to the magnetic zone boundary at (101) as shown in Fig. 14. However, one has to be cautious as due to the twinned nature of the sample at **Q** = (101), there will also be a contribution of the other twin domains (twin II) for which this **Q** is equivalent to the magnetic zone center (011) [see Fig. 1(e)]. The fact that we see a clear c dispersion arises from the dominating domain fraction of twin I. However, at (101) for twin I we probe the transverse fluctuation along the b axis, whereas at (011) for twin II the a axis fluctuation is detected. A sizable in-plane anisotropy can therefore hide an even steeper c dispersion in Fig. 15. In comparison to $LaSrFeO_4$ the absence of magnetic scattering below the single peaks visible in Fig. 13 proves that the transverse excitations are gapped, however, the

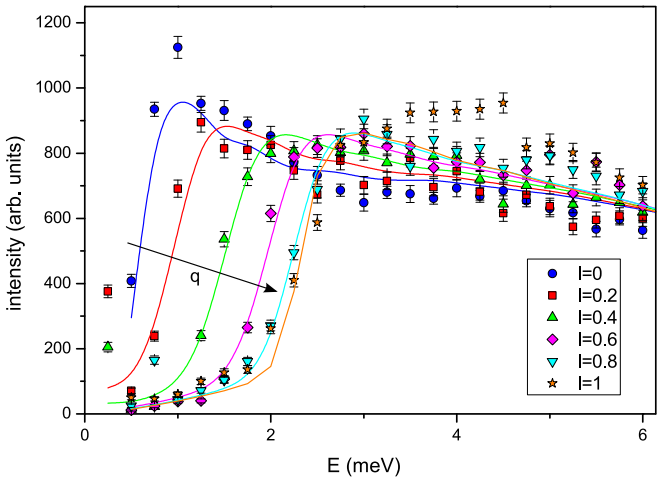

FIG. 15. (Color online) Constant-**Q** scans at $Q = (10l)$ and $T = 10$ K for different l values documenting the weakly dispersive vertical mode.

partial twinning does not allow us to quantify the respective gaps without the use of neutron polarization analysis.

Although the magnon dispersion could only be studied on sample $S2$ we may safely assume that the obtained interaction parameter is fully representative for $PrCaFeO_4$ in the two magnetic phases. The anisotropy gaps and parameters, however, can be attributed only to single-crystalline stoichiometric $PrCaFeO_4$, because the real structure possesses a strong impact on these much smaller energy scales.

V. CONCLUSION

We have presented a comprehensive study using x-ray and neutron diffraction as well as inelastic neutron scattering together with macroscopic measurements on three different $PrCaFeO_4$ samples. All samples show experimental proof for two structural phase transitions. Macroscopic methods and neutron diffraction reveal a magnetic spin-flop transition in the high-quality single-crystal sample $S2$, which is also observed by neutron diffraction experiments on the polycrystalline sample $S3$. All phase transitions are therefore intrinsic properties of $PrCaFeO_4$, but their temperatures and especially the temperature regime of the magnetic transitions are very sensitive to the sample quality (see Table IV for a comparison). The structural investigation suggests that the stoichiometric single crystal exhibits a rather sharp spin-flop transition, whereas the transition broadens substantially and shifts to higher temperature in a powder sample.

TABLE IV. Comparison of the structural ($T_{S,1}$: $I4/mmm \rightarrow Bmeb$, $T_{S,2}$: $Bmeb \rightarrow Pccn$) and magnetic phase transition temperatures (T_{SF}: spin-flop transition temperature) for the oxygen-deficient single-crystal sample $S1$, the stoichiometric single-crystal sample $S2$, and the powder sample $S3$. A dash means that the technique which revealed the phase transition was not applied to that particular sample or that it could not be observed.

	$S1$	$S2$	$S3$
$T_{S,1}$ (K)	783	783	–
$T_{S,2}$ (K)	–	240	300
T_N (K)	–	>300	$\geqslant 330$
T_{SF} (K)	–	42	75–175

The analysis of the magnon dispersion in $PrCaFeO_4$ reveals a nearest-neighbor antiferromagnetic interaction, which is fully comparable to that in $LaSrFeO_4$. The tilting of the FeO_6 octahedra by about 8 degrees does not imply a significant reduction of this exchange parameter. In contrast to $LaSrFeO_4$, the spin-wave spectrum is fully gapped in $PrCaFeO_4$, which is a direct consequence of the orthorhombic distortion. In the tetragonal layered system only a higher-order in-plane anisotropy is possible but apparently too small to be detected. Combining the elastic and inelastic studies we may identify the a axis as the magnetic hard axis in $PrCaFeO_4$.

A further interesting aspect in $PrCaFeO_4$ concerns the relief of geometrical frustration due to the orthorhombic distortion. As the nearest-neighbor interactions within the a-b plane are completely satisfied, the orthorhombicity does not have a sizable influence on the in-plane spin-wave dispersion. However, every Fe spin has four antiparallel neighbors in the a-c plane and four parallel neighbors in the b-c plane which create a zero effective field as long as the symmetry is tetragonal, as is the case for $LaSrFeO_4$. The orthorhombic distortion, however, lifts this frustration and thereby induces a finite interlayer spin-wave dispersion. In most quasi-isostructural materials like cuprates, nickelates, or manganites, such effects still remain very small and no interlayer dispersion was reported [26–29]. It is therefore remarkable that a finite interlayer dispersion can clearly be observed in $PrCaFeO_4$.

ACKNOWLEDGMENT

This work was supported by the Deutsche Forschungsmeinschaft through the Sonderforschungsbereich 608.

[1] S. N. Ruddlesden and P. Popper, Acta Crystallogr. **10**, 538 (1957).
[2] S. Jin, T. H. Tiefel, M. McCormack, R. A. Fastnacht, R. Ramesh, and L. H. Chen, Science **264**, 413 (1994).
[3] K. Yamada, M. Matsuda, Y. Endoh, B. Keimer, R. J. Birgeneau, S. Onodera, J. Mizusaki, T. Matsuura, and G. Shirane, Phys. Rev. B **39**, 2336 (1989).
[4] J. Rodríguez-Carvajal, M. T. Fernandez-Díaz, and J. L. Martínez, J. Phys. Condens. Matter **3**, 3215 (1991).
[5] M. Imada, A. Fujimori, and Y. Tokura, Rev. Mod. Phys. **70**, 1039 (1998).
[6] M. Cwik, M. Benomar, T. Finger, Y. Sidis, D. Senff, M. Reuther, T. Lorenz, and M. Braden, Phys. Rev. Lett. **102**, 057201 (2009).

[7] H. Ulbrich, D. Senff, P. Steffens, O. J. Schumann, Y. Sidis, P. Reutler, A. Revcolevschi, and M. Braden, Phys. Rev. Lett. **106**, 157201 (2011).
[8] I. A. Zaliznyak, J. P. Hill, J. M. Tranquada, R. Erwin, and Y. Moritomo, Phys. Rev. Lett. **85**, 4353 (2000).
[9] J. L. Soubeyroux, P. Courbin, L. Fournes, D. Fruchart, and G. le Flem, J. Solid State Chem. **31**, 313 (1980).
[10] C. Bansal, H. Kawanaka, H. Bando, A. Sasahara, R. Miyamoto, and Y. Nishihara, Solid State Commun. **128**, 197 (2003).
[11] N. Qureshi, H. Ulbrich, Y. Sidis, A. Cousson, and M. Braden, Phys. Rev. B **87**, 054433 (2013).
[12] J. Reul, L. Fels, N. Qureshi, K. Shportko, and M. Braden, and M. Grüninger Phys. Rev. B **87**, 205142 (2013).
[13] S. Oyama, M. Wakeshima, Y. Hinatsu, and K. Ohayama, J. Phys. Condens. Matter **16**, 1823 (2004).
[14] S. Oyama, M. Wakeshima, Y. Hinatsu, and K. Ohayama, J. Phys. Condens. Matter **16**, 8429 (2004).
[15] K. Oka and H. Unoki, Japanese Association of Crystal Growth **14**, 183 (1987).
[16] J. Rodríguez-Carvajal, Physica B **192**, 55 (1993).
[17] A. C. Larson, in *Crystallographic Computing*, edited by F. R. Ahmed, S. R. Hall, and C. P. Huber (Copenhagen, Munksgaard, 1970), pp. 291–294.
[18] R. L. White, J. Appl. Phys. **40**, 1061 (1969).
[19] W. Slawinski, R. Przeniosko, I. Sosnowska, and E. Suard, J. Phys. Condens. Matter **17**, 4605 (2005).
[20] H. Wu, S. Cao, M. Liu, Y. Cao, B. Kang, J. Zhang, and W. Ren, Phys. Rev. B **90**, 144415 (2014).
[21] P. J. Hirschfeld, M. M. Korshunov, and I. I. Mazin, Rep. Prog. Phys. **74**, 124508 (2011).
[22] N. Qureshi, P. Steffens, S. Wurmehl, S. Aswartham, B. Büchner, and M. Braden, Phys. Rev. B **86**, 060410(R) (2012).
[23] F. Waßer, A. Schneidewind, Y. Sidis, S. Wurmehl, S. Aswartham, B. Büchner, and M. Braden, Phys. Rev. B **91**, 060505(R) (2015).
[24] A. Zheludev, RESLIB 3.4c (Oak Ridge National Laboratory, Oak Ridge, TN) (2006).
[25] W. Marshall and S. Lovesey, *Theory of Thermal Neutron Scattering* (Oxford University Press, Oxford, 1971).
[26] R. Coldea, S. M. Hayden, G. Aeppli, T. G. Perring, C. D. Frost, T. E. Mason, S.-W. Cheong, and Z. Fisk, Phys. Rev. Lett. **86**, 5377 (2001).
[27] K. Nakajima, K. Yamada, S. Hosoya, T. Omata, and Y. Endoh, J. Phys. Soc. Jpn. **62**, 4438 (1993).
[28] S. Larochelle, A. Mehta, L. Lu, P. K. Mang, O. P. Vajk, N. Kaneko, J. W. Lynn, L. Zhou, and M. Greven, Phys. Rev. B **71**, 024435 (2005).
[29] D. Senff, F. Krüger, S. Scheidl, M. Benomar, Y. Sidis, F. Demmel, and M. Braden, Phys. Rev. Lett. **96**, 257201 (2006).